Supporting Information

Excessive Se on RuSe₂ nanocrystals to accelerate water dissociation for enhanced electrocatalytic hydrogen evolution reaction

Kefeng Wang,[a] Bin Li,[b] Wei Wei,[*a] Jingge Wang,[c] Qi Shen[b] and Peng Qu[*a, b]

[a] Henan Engineering Center of New Energy Battery Materials, Henan Key Laboratory of Biomolecular Recognition and Sensing, College of Chemistry and Chemical Engineering, Shangqiu Normal University, Shangqiu 476000, Henan, China

[b] College of Chemistry and Molecular Engineering, Zhengzhou University, Zhengzhou 450001, China

[c] School of Physics and Engineering, Henan University of Science and Technology, Luoyang 471023, China

Experimental Section

Materials: $RuCl_3$ and Se powder were purchased from Energy Chemical Ltd. (Shanghai, China). Hydrazine hydrate (85 wt%) and KOH were purchased from Aladdin Ltd. (Shanghai, China). Commercial 20% Pt/C, RuO_2 catalysts and Nafion ethanol solution (5 wt%, DuPont) were purchased from Shanghai Macklin Biochemical Co., Ltd. All chemical reagents used were of analytical grade and used without further purification. Carbon fiber paper (CFP) was bought from Shanghai Hesen Corp.

Synthesis of Ru_xSe: Ru_xSe nanocrystals were synthesized through a facial hydrothermal method. Typically, 0.06 g Se powder and 0.0518 g $RuCl_3$ were mixed in deionized water (35 mL). After vigorous stirring for 10 min, 2 mL hydrazine hydrate (85 wt%) was dropped into the above solution under constant stirring. The resulting solution was transferred into a 50 mL Teflon−lined autoclave, and the autoclave was sealed and maintained at 120 °C for 12 h. After naturally cooled to room temperature, the precipitate was collected and washed thoroughly with deionized water and ethanol, and finally dried in vacuum at 60 °C overnight. The obtained samples were further pyrolyzed at different temperature (300 °C, 400°C, 500 °C and 600 °C) for 2 h in an Ar atmosphere to obtain Ru_xSe nanocrystals.

Material characterizations: X-ray diffraction (XRD) patterns were recorded at room temperature on a Bruker D8 Advance X-ray diffractometer using a Cu Kα radiation (λ=1.5416 Å) with 2θ scan range between 10° and 80°. Transmission electron microscopy (TEM) images, high-resolution TEM (HRTEM) images, energy dispersive X-ray (EDX) elemental mappings and EDX spectra were collected using a FEI Tecnai G2 F20 field-emission transmission electron microscopy equipped with an EDX detector. X-ray photoelectron spectroscopy (XPS) measurements were carried out with a ThermoFisher K-Alpha X-ray photoelectron spectrometer with an Al Kα source. All the binding energies were calibrated to the standard C 1s emission signal (284.8 eV) of the contaminant carbon during the measurement. Brunauer–

Emmett–Teller (BET) measurements were carried out using a Surface area and Porosity Analyzer (ASAP2020).

Preparation of catalyst electrodes: Different catalysts including 20% Pt/C and RuO_2 were loaded on carbon fiber paper (CFP) through a drop-casting method. Briefly, 10 mg of the catalyst were dispersed in 480 μL of water–ethanol solution at volume ratio of 250:230. Then 20 μL of Nafion solution (5 wt%, DuPont) was added. The obtained mixture was ultra-sonicated for 3 h to form a homogenous ink. Then 50 μL catalyst ink was dropped onto a piece of carbon fiber paper (CFP, 1 cm × 1cm) and left to dry at room temperature overnight. The catalyst loading was 1 mg cm^{-2}.

Electrochemical measurements: All the electrochemical measurements were carried out with a CHI660E electrochemical analyzer using a standard three-electrode cell system. The catalyst electrode, Hg/HgO electrode and a graphite rod were used as the working electrode, reference electrode and counter electrode, respectively. A KOH aqueous solution (1 M) was used as the electrolyte during the whole measurement. Prior to the test, the electrolyte was purged with high-purity N_2 for at least 30 min to remove dissolved O_2. Polarization curves were recorded by conducting linear sweep voltammetry (LSV) measurements with a potential window of -0.8 V~-1.6 V vs Hg/HgO at a scan rate of 2 mV/s. All the potentials were calibrated with respect to a reversible hydrogen electrode (RHE) using $E_{RHE} = E_{Hg/HgO} + 0.935$. The calibration was performed using two pieces of Pt foil (1 cm×1cm) in a high-purity H_2-saturated electrolyte. In order to reveal the intrinsic electrocatalytic behavior of the catalysts, 90% IR compensations were applied to all the polarization curves based on the ohmic resistance of the solution determined by electrochemical impedance spectroscopy (EIS). EIS tests were carried out with the frequency ranging from 100 mHz to 100 kHz and a 5 mV amplitude. The electrochemical stability test of the catalyst was conducted by continuously cyclic voltammetry (CV) measurement between -0.8 V~ -1.3 V (vs Hg/HgO) for 3000 cycles at a scan rate of 100 mV s^{-1}, and the polarization curves before and after CV measurement were recorded.

Chronoamperometric measurement was conducted for 18 h at an overpotential of 45 mV to monitor the long-term i-t response for the HER test. The volume of H_2 produced under a constant current density at different time was measured using a gas chromatography.

Computational Method: All the density functional theory (DFT) calculations were performed by using Vienna Ab-initio Simulation Package[1,2](VASP) under the Projected Augmented Wave[3](PAW) method. The revised Perdew-Burke-Ernzerhof (RPBE) functional was used to describe the exchange and correlation effects, since it has been proved to provide useful trend in computing adsorption energies.[4-6] In all the calculations, the cutoff energy was set to be 500 eV. To mimic the Se-enriched environment, we added a Se dimer on the (210) surface of $RuSe_2$. The Monkhorst-Pack grids[7] were set to be 6×3×1 for (210) surface, respectively. At least 18 Å vacuum layer was applied in z-direction of the slab models, preventing the slabs from vertical interactions.

The descriptor proposed by Norskov et al. was used to describe the HER activity on a given catalyst surface, where the free energy of hydrogen adsorption (ΔG_{H*}) was considered as the key parameter determining the HER activity.[8] For HER in acidic solutions, it is a two-step process and involves only one reaction intermediate, the chemisorbed H atom. The free energy of the adsorbed hydrogen is defined as:

$$\Delta G_{H*} = \Delta E_H + \Delta E_{ZPE} - T\Delta S_H$$

where ΔE_H is the hydrogen binding energy, ΔE_{ZPE} is the zero-point energy difference between adsorbed hydrogen and gaseous hydrogen, and $T\Delta S$ is the corresponding entropy difference between these two states. According to previous studies, here we used a 0.24 eV value to represent the correction of zero-point energy and entropy of hydrogen state.
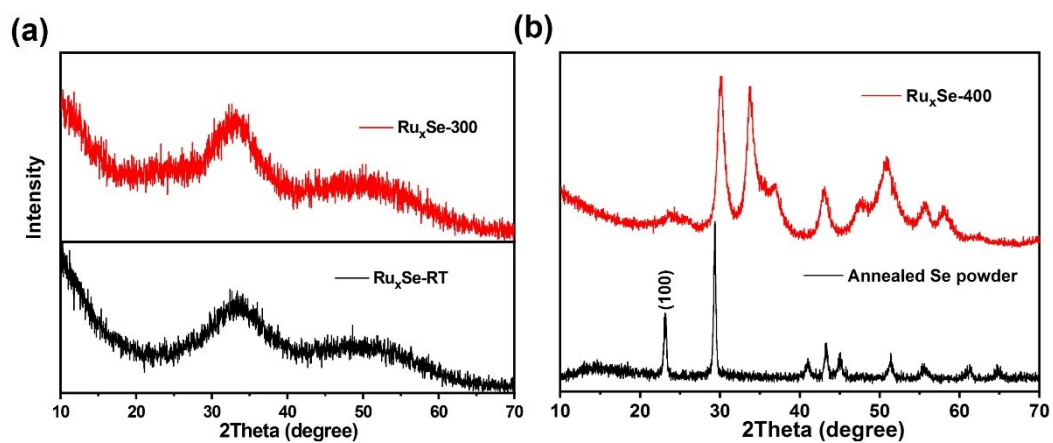
Fig. S1 Comparision of XRD patterns of (a) Ru_xSe-RT and Ru_xSe-300 and (b) RuSe-400 and annealed Se powder.
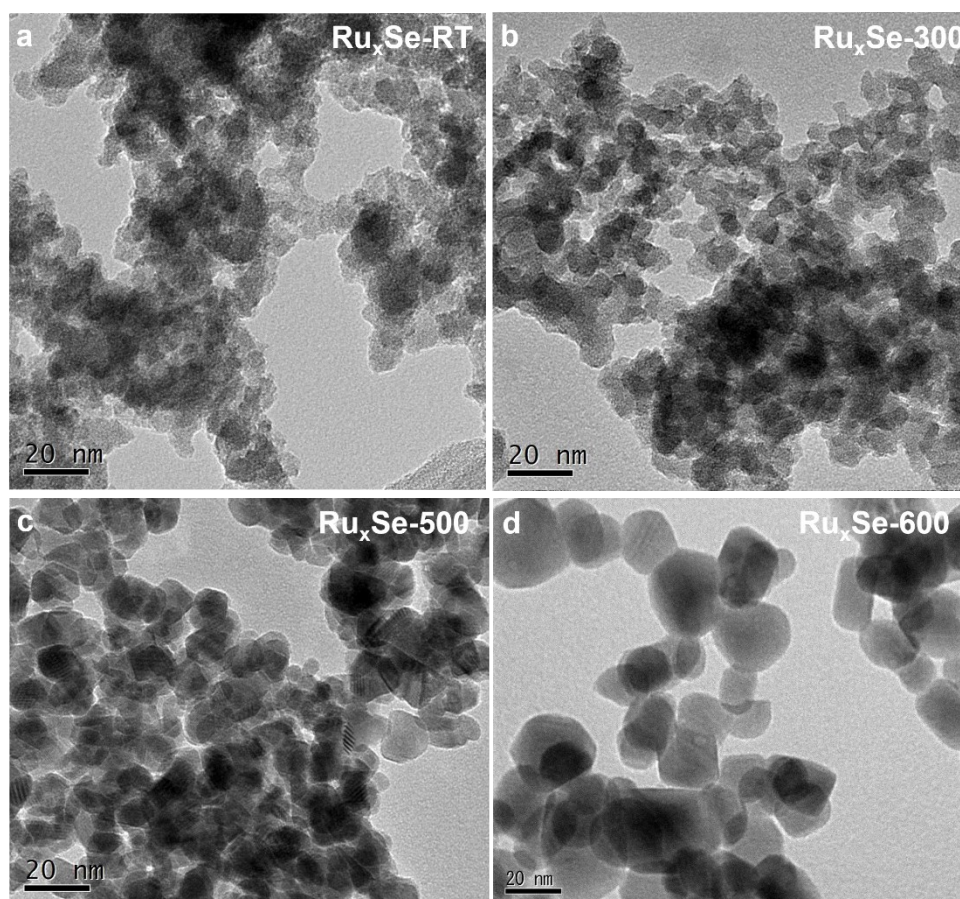

Fig. S2 TEM images of the pristine Ru_xSe (Ru_xSe-RT) and the samples calcinated at different temperatures.
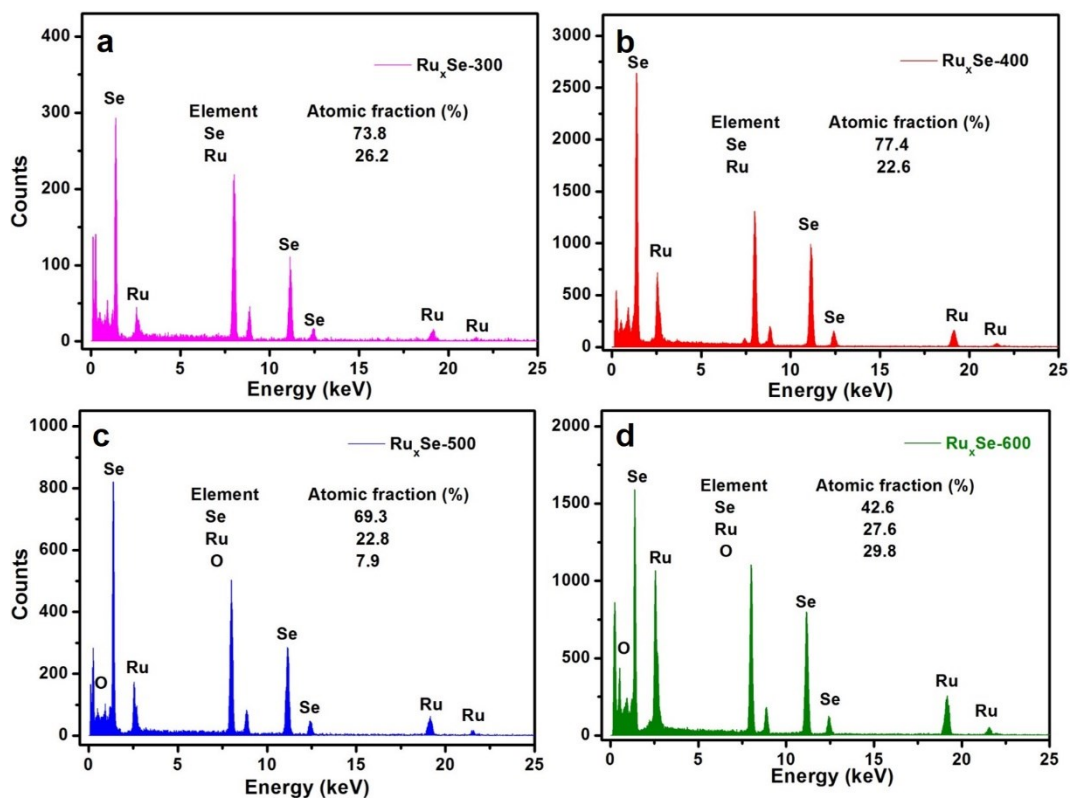
Fig. S3 EDX spectra and the corresponding elemental composition of the Ru$_x$Se nanocrystals obtained at different temperature.
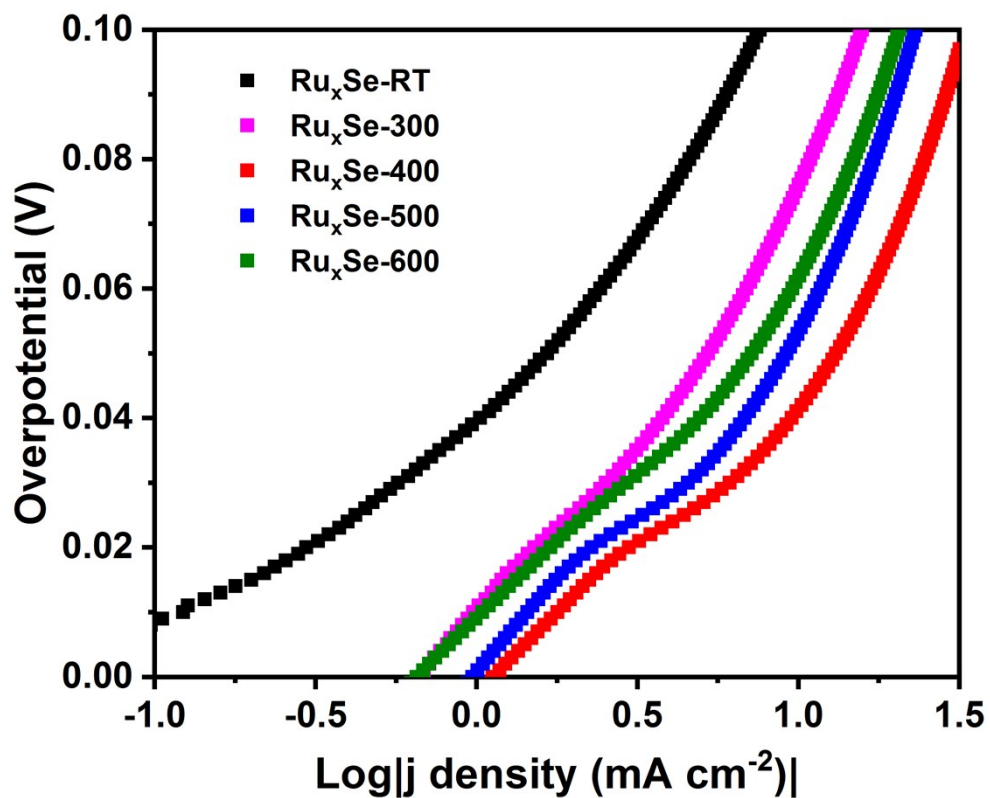

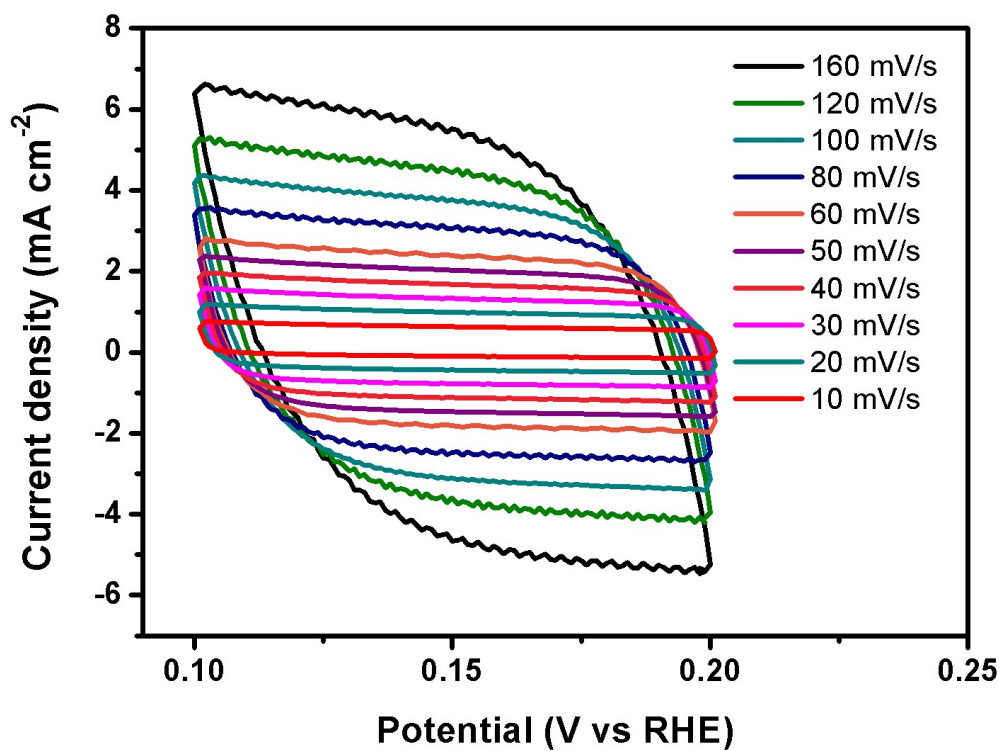**Fig. S4** Tafel plots of Ru$_x$Se nanocrystals calcinated at different temperatures.

Fig. S5 yclic voltammetry curves of Ru$_x$Se-400 at different scan rates ranging from 10 mV/s to 160 mV/s.
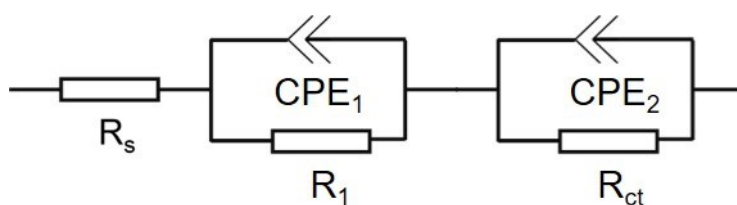

Fig. S6 The equivalent circuit used to fit the Nyquist plots for different catalysts recorded at a bias voltage of -200 mV vs RHE.
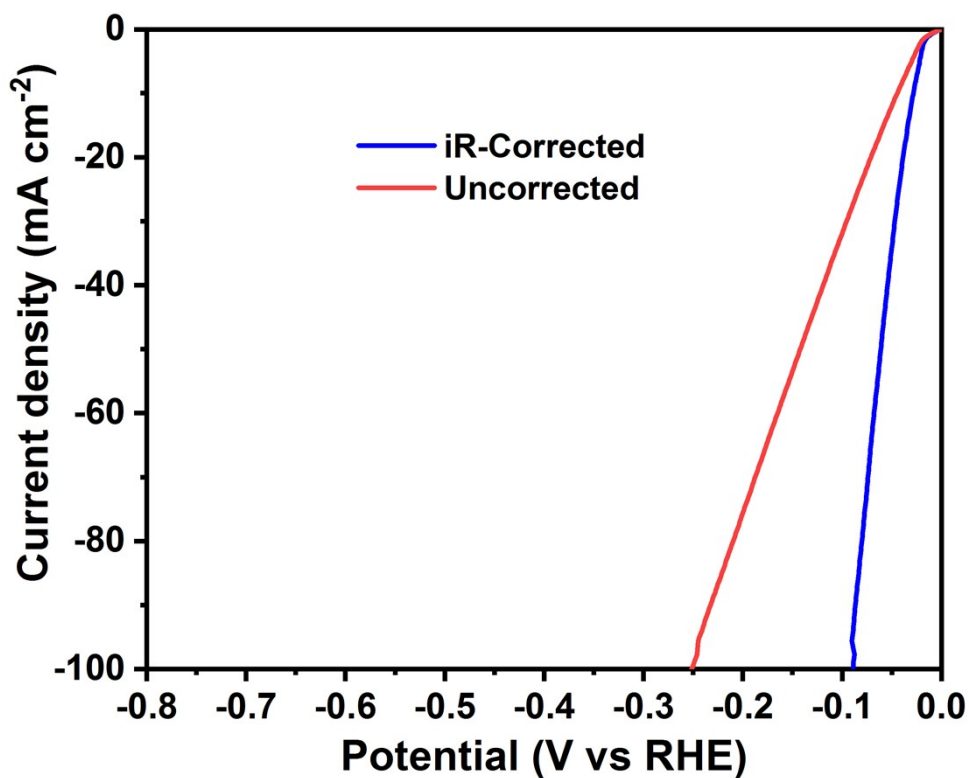
Fig. S7 Polarization curves of Ru$_x$Se-400 with and without IR-correction. The IR-correction was based on the resolution resistance (1.8 Ω) measured by EIS at an overpotential of 100 mV.
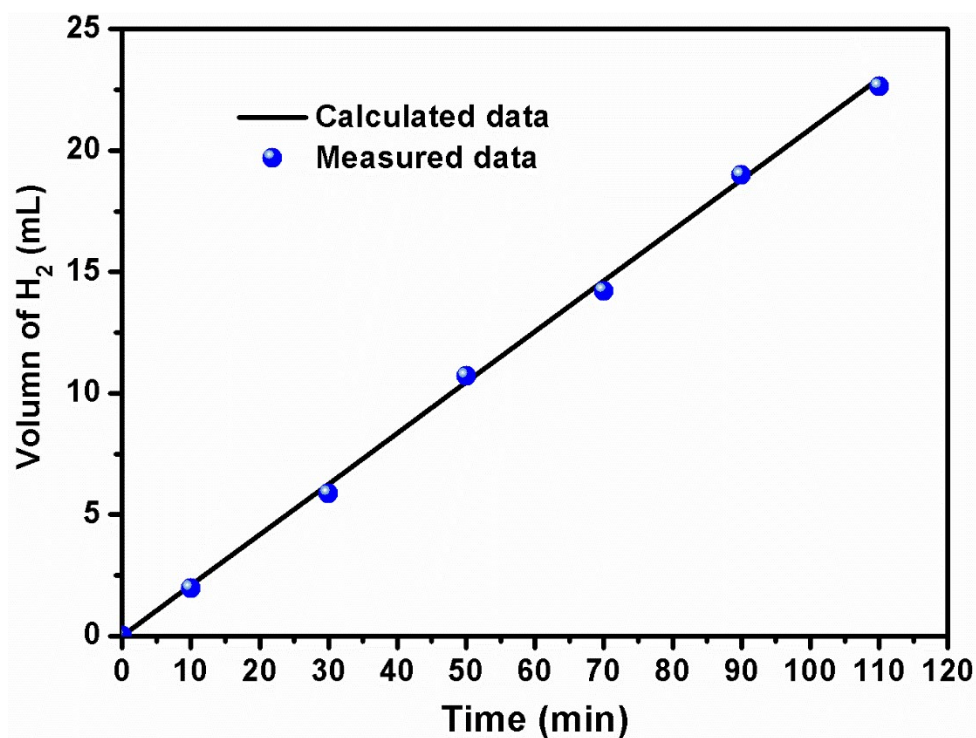
Fig. S8 Experimentally measured H_2 production and theoretically calculated amount by operating HER under a constant current density of -20 mA cm^{-2}
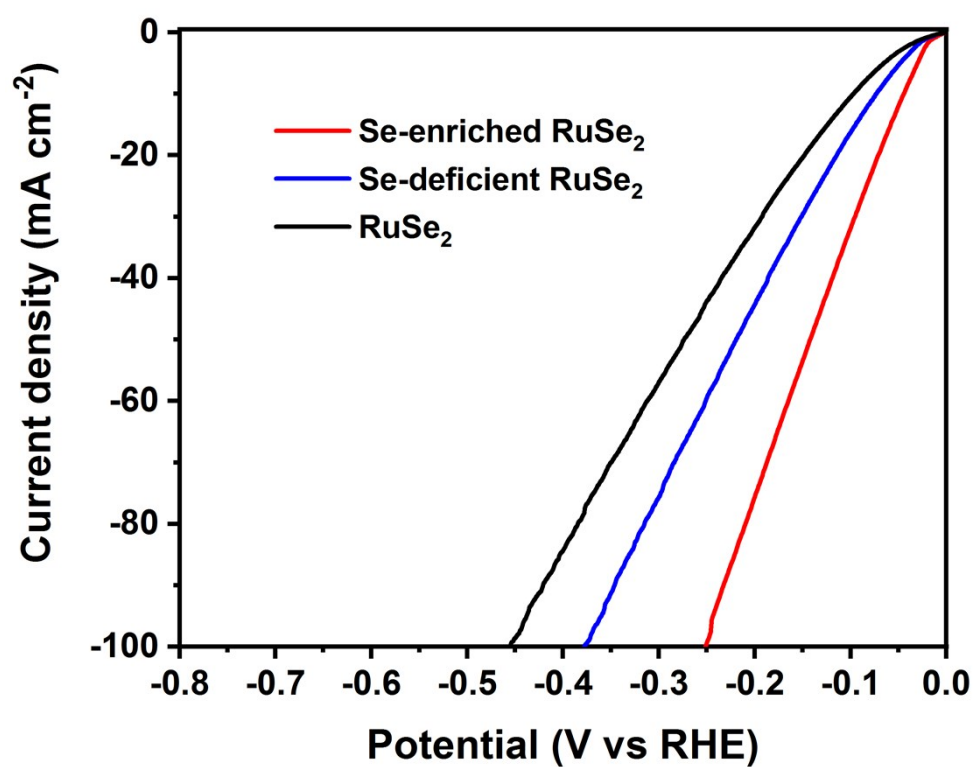

Fig. S9 Comparison of HER performances of Se-enriched RuSe$_2$, RuSe$_2$ and Se-deficient RuSe$_2$ nanocrystals.
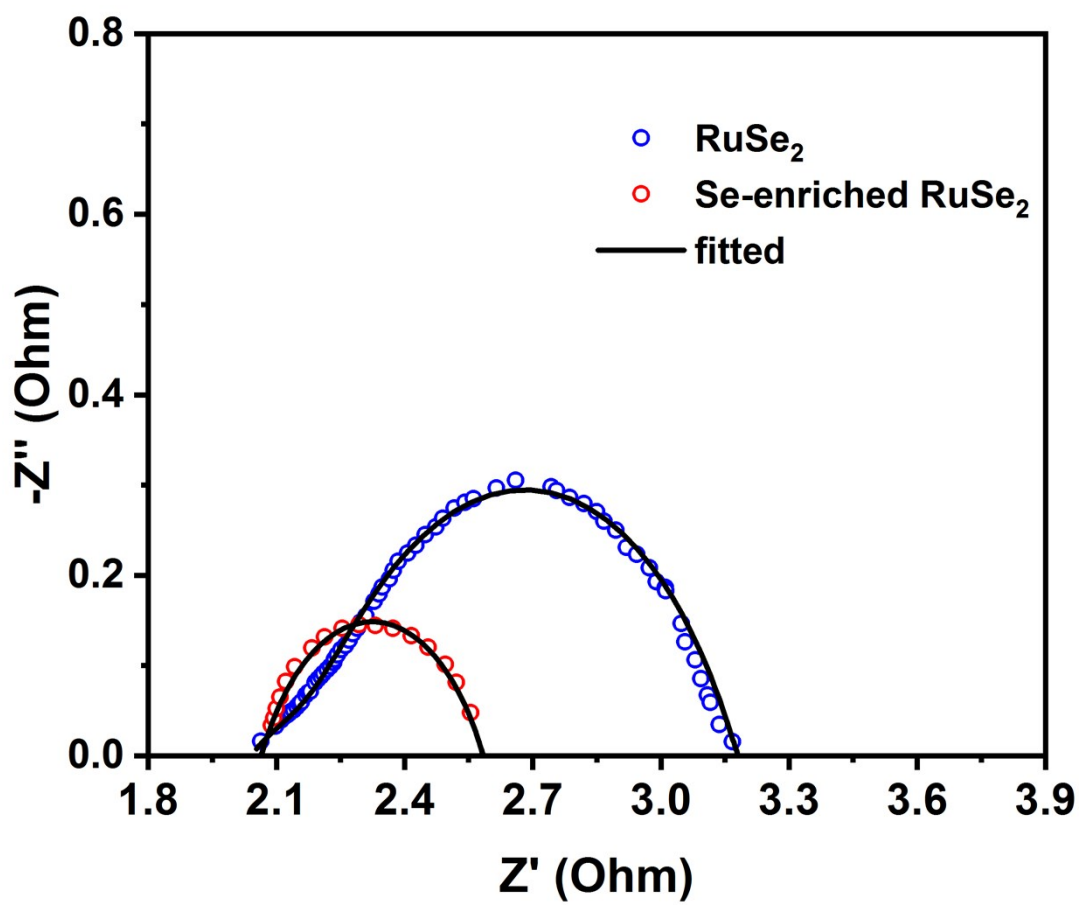
Fig. S10 EIS spectra of Se-enriched $RuSe_2$ and $RuSe_2$ carried out at an overpotential of -200 mV
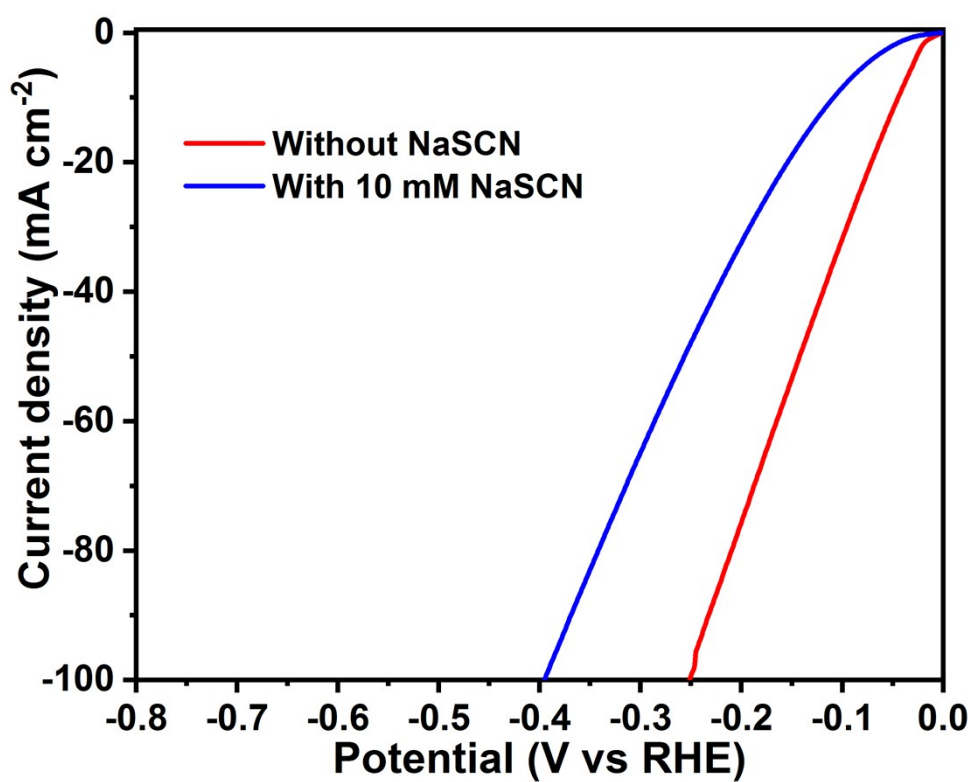
Fig. S11 HER polarization curves of Ru_xSe-400 in 1 M KOH electrolyte with and without 10 mM NaSCN.
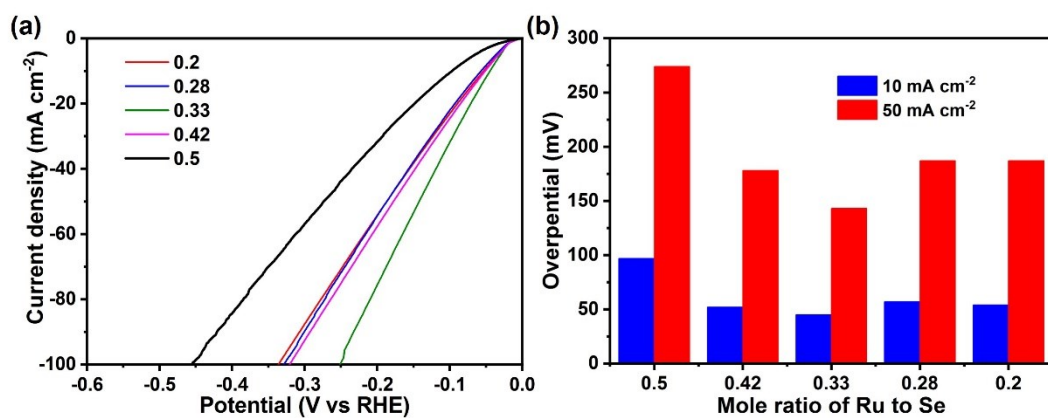
Fig. S12 (a) HER polarization curves of Ru_xSe-400 with differet x values and (b) the overpotentials at 10 mA cm^{-2} and 50 mA cm^{-2} for different catalysts.
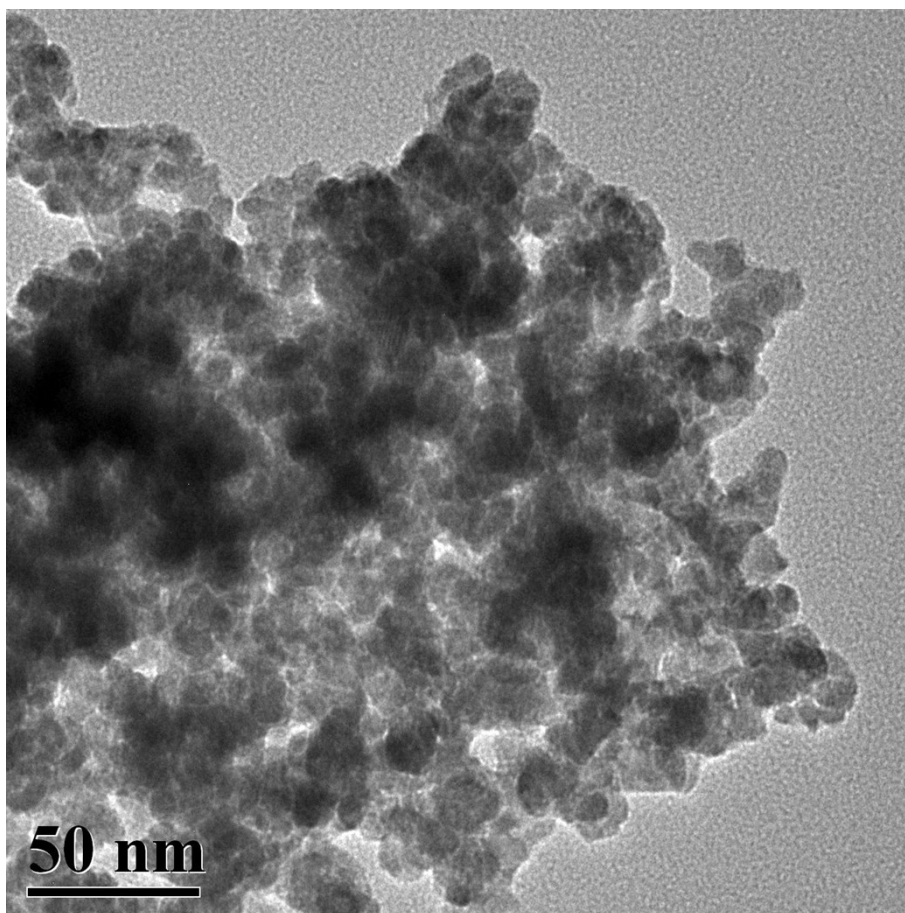
Fig. S13 TEM image of Ru$_x$Se-400 after long-time stability test.
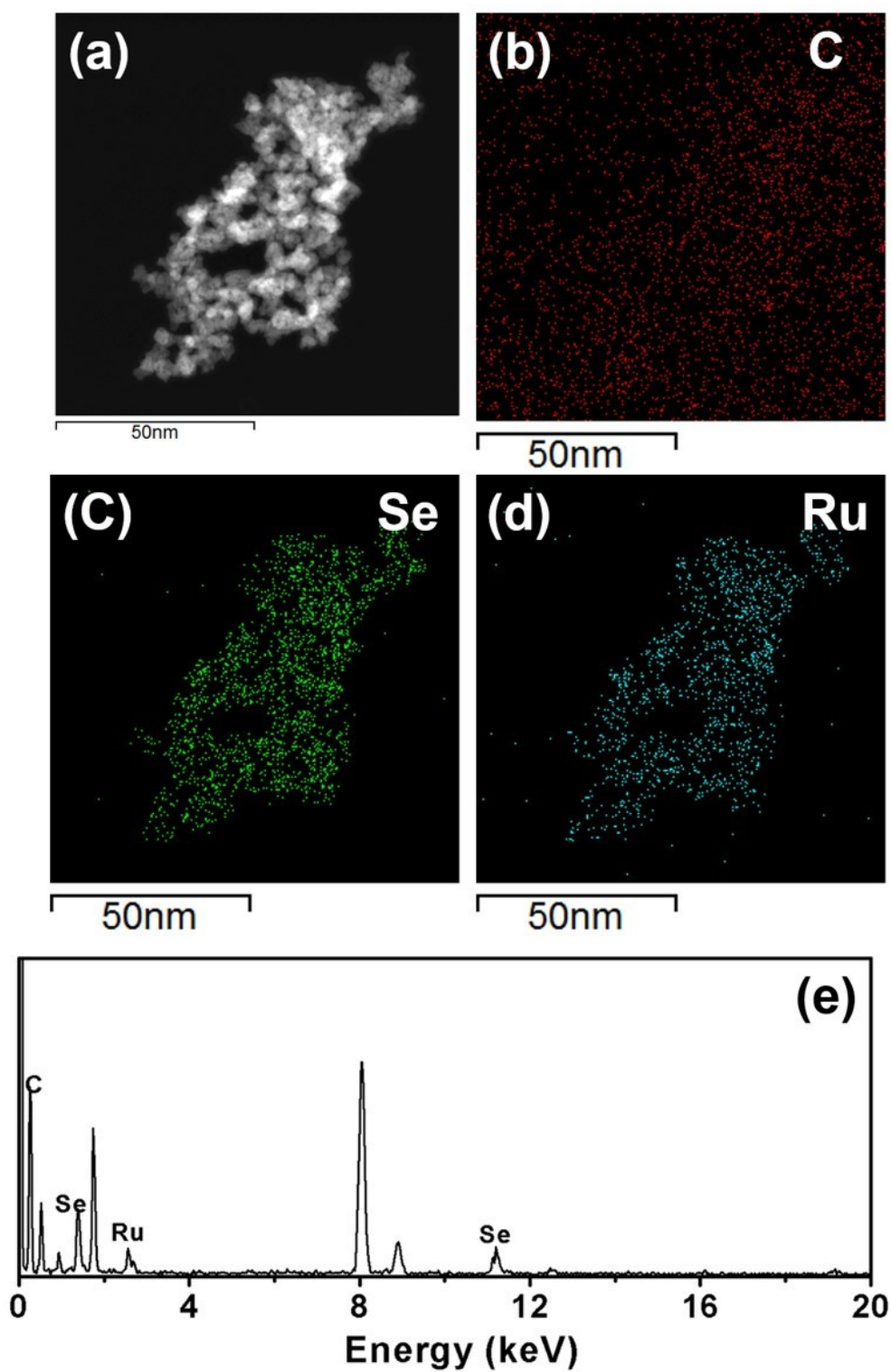
Fig. S14 STEM (a) and elemental mapping images (b, c, d) and of EDX spectrum (e) of Ru$_x$-400 after long-time stability test.
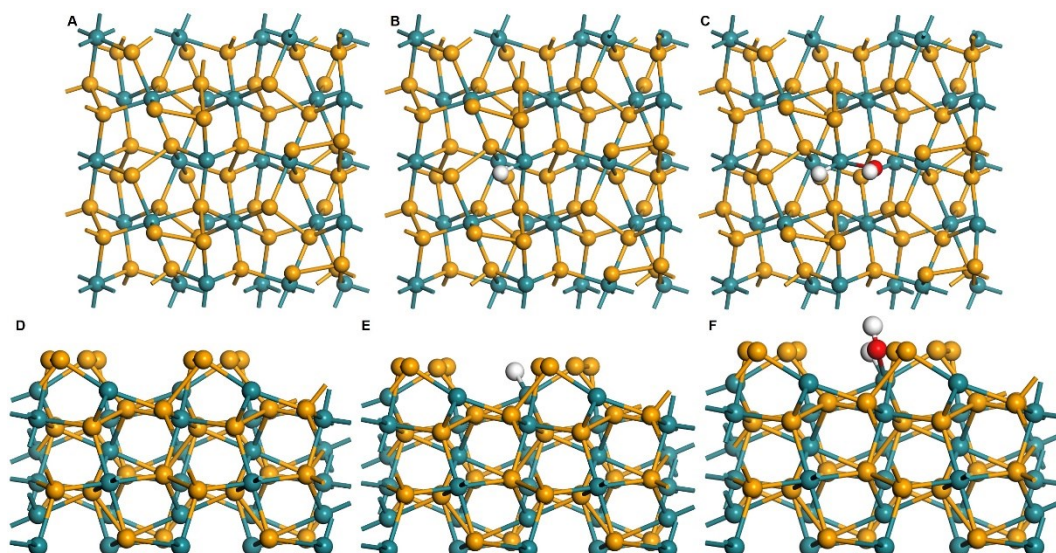
Fig. S15 (A, B, C) Top views and (D, E, F) side views of calculated configurations for the original state, H* and H−OH* adsorption states on RuSe$_2$ (210). The dark green, yellow, white and red spheres correspond to Ru, Se, O and H atoms.

Fig. S16 (A, B, C) Top views and (D, E, F) side views of calculated configurations for the original state, H* and H−OH* adsorption states on Se-enriched RuSe$_2$ (210). The dark green, yellow, white and red spheres correspond to Ru, Se, O and H atoms. While the blue spheres represent the surface adsorbed Se atoms.

Table S1 The elemental contents in Ru_xSe-T by ICP-AES.

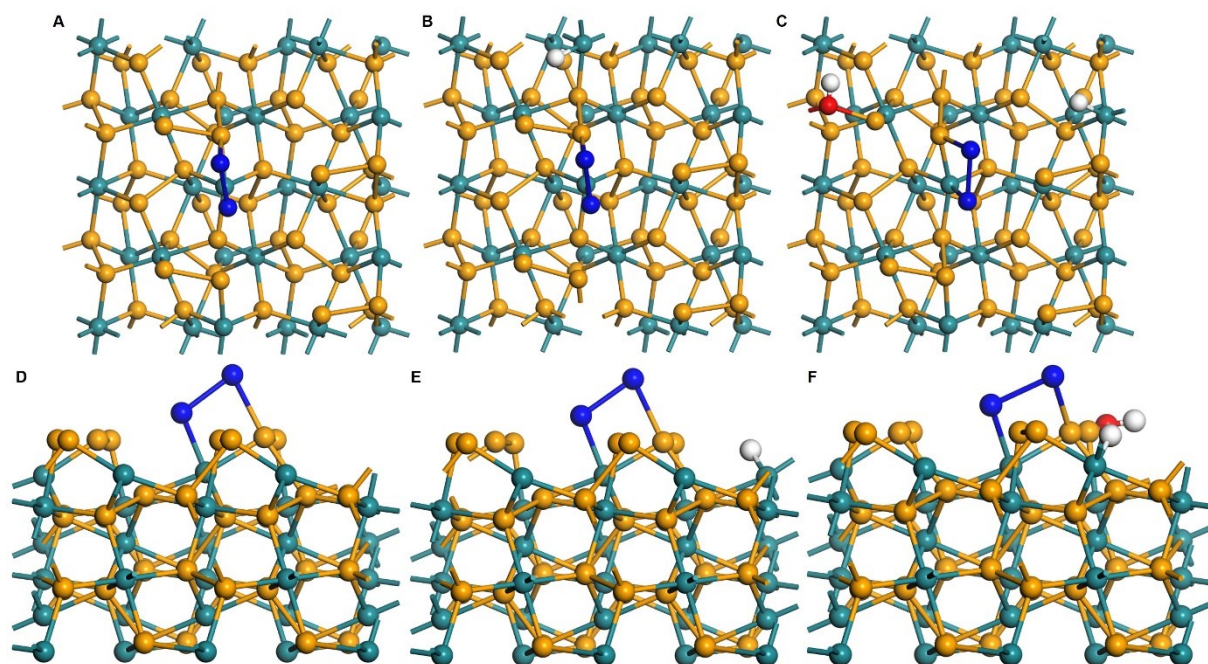| Catalyst	Ru (wt.%)	Se (wt.%)
Ru_xSe-RT	32.09	68.22
Ru_xSe-300	28.47	67.97
Ru_xSe-400	27.85	63.50
Ru_xSe-500	32.85	60.77
Ru_xSe-600	30.75	48.43

Table S2 The overpotential at the current density of 10 mA/cm^2 (with IR-compensation), and Tafel slopes for Ru-based HER electrocatalysts in alkaline media.

Catalysts	η@10 mA cm^{-2} (mV)	Tafel slope (mV dec^{-1})	Ref.
Ru_xSe-400	28.5	31.9	This work
Ru-ZIF-900	51.6	78.4	J. Mater. Chem. A, 2020, 8, 3203
single Ru atoms anchored on MoS_2 nanosheets array	41	114	Appl. Catal., B, 2019, 249, 91
Ru-NiFe-P nanosheets on 3D self-supported nickel foam	44	31.5	Appl. Catal., B, 2020, 263, 118324
Ruthenium nanoparticles anchored on graphene hollow nanospheres	24.4	34.8	Inorg. Chem., 2020, 59, 930
ruthenium nanoparticles dispersed on N-doped carbon hollow nanospheres	28.8	32.7	Chem. Commun., 2020, 56:6802
Ru nanoparticles highly dispersed on carbon supports	25	33	Adv. Energy Mater. 2018, 1801698
Ru nanoparticles anchored on the graphene nanoplatelets	22	28	Adv. Mater. 2018, 1803676
Ru/Cu-doped RuO_2 complex embedded in amorphous carbon skeleton	28	35	Small 2018, 1803009
Cactus-like hollow $Cu_{2-x}S$@Ru nanoplates	82	48	Small 2017, 13, 1700052
hierarchical 4H/fcc Ru Nanotubes	23	29.4	Small 2018, 1801090
Ru_2P nanoparticle decorated P/N-doped carbon nanofibers	50	66	ACS Applied Energy Materials 2018, 1, 3143
RuO_2 nanoparticles on nitrogen-doped Carbon Matrix	40	47	ACS Sustainable Chemistry &

Catalysts			Ref.
Ru$_2$P nanoparticles	54	29	Engineering 2018, 6, 11529 ChemSusChem 2018, 11, 1-7
RuP$_2$ encapsulated in N, P dual-doped carbon	52	69	*Angew. Chem. Int. Ed.* **2017**, *56*, 11559.
Ruthenium-cobalt nanoalloys encapsulated in nitrogen-doped graphene	28	31	*Nat.Commun.*, **2017**, *8*, 14969.
Ru decorated with NiCoP	52	50	*Chem. Commun.*, **2017**, *53*, 13153.
NiRu nanoalloys encapsulated in nitrogen-doped carbon	32	64	*J. Mater. Chem. A*, **2018**, *6*, 1376.
RuPx nanoparticles encapsulated in uniform N,P-codoped hollow carbon nanospheres	74	70	*ChemSusChem*, **2018**, *11*, 743.
Ru nanocrystal supported N-doped graphene	40	76	*Sustainable Energy Fuels*, **2017**, *1*, 1028.
Self-crosslinking carbon dots loaded ruthenium dots	29	57	*Nano Energy*, **2019**, *65*: 104023
Ru nanoparticles (Ru NPs) catalyst supported on carbon quantum dots	65	63	*Mater. Chem. Front.*, **2020**, *4*: 277-284

Table S3 HER activity of transition metal selenides in alkaline media.

Catalysts	η@10 mA cm^{-2} (mV)	Tafel slope (mV dec^{-1})	Ref.
Ni$_{0.89}$Co$_{0.11}$Se$_2$ mesoporous nanosheet networks on nickel foam	85	52	*Adv. Mater.*, **2017**, *29*, 1606521.
Co-doped NiSe$_2$ nanoparticles on Ti foil	64	63	*Nanoscale*, **2016**, *8*, 3911.
NiSe nanowire on nickel foam	96	120	*Angew. Chem. Int. Ed.* **2015**, *54*, 9351.
porous NiSe$_2$ nano-wrinkles on nickel foam	166	92.3	*ACS Sustainable Chem. Eng.*, **2018**, *6*, 2231.
cubic phase CoSe$_2$ on carbon cloth	190	85	*Adv. Mater.* **2016**, *28*, 7527.
Co$_7$Se$_8$	472	59.1	*ACS Appl. Mater.*

			Interfaces, **2016**, *8*, 17292.
porous $NiSe_2$ nanosheets on carbon paper	184	77	*Chem. Mater.*, **2015**, *27*, 5702.
NiSe nanoparticles decorated reduced graphene oxide-polyimide/carbon nanotube film	270	61	*Electrochim. Acta*, **2017**, *243*, 291.
Textured $NiSe_2$ Film	170	107	*Sci. Rep.*, **2017**, *7*, 2401.
$CoSe_2$ Nanocrystals	520	126	*ACS Appl. Mater. Interfaces,* **2016**, *8*, 5327.
$NiSe_2$ Nanocrystals	540	139	
NiFe layered double hydroxide-NiSe	163	70	*ACS Appl. Mater. Interfaces,* **2017**, *9*, 33766.
NiSe@CoP core–shell nanowire arrays	91	55	*Catal. Sci. Technol.*, **2018**, *8*, 128.
Mo, S-codoped NiSe/NF	88	82	*J. Mater. Chem. A*, **2017**, *5*, 20588.
amorphous CoSe film on a Ti mesh	121	84	*Chem. Commun.*, **2015**, *51*, 16683.
$NiSe/Ni_3Se_2/NF$	92	101.2	*Adv. Mater. Interfaces* **2018**, *5*, 1701507

References

1. G. Kresse and J. Hafner, *Physical Review B* 1994, **49**, 14251.

2. G. Kresse and J. Furthmüller, *Physical Review B* 1996, **54**, 11169.

3. P. E. Blöchl, *Physical Review B* 1994, **50**, 17953.

4. J. P. Perdew, K. Burke and M. Ernzerhof, *Phys. Rev. Lett.* 1996, **77**, 3865.

5. Y. Zhang and W. Yang, *Phys. Rev. Lett.* 1998, **80**, 890.

6. B. Hammer, L. B. Hansen and J. K. Nørskov, *Physical Review B* 1999, **59**, 7413.

7. H. J. Monkhorst and J. D. Pack, *Physical review B* 1976, **13**, 5188.

8. J. K. Nørskov, T. Bligaard, A. Logadottir, J. Kitchin, J. G. Chen, S. Pandelov and U. Stimming, *J. Electrochem. Soc.* 2005, **152**, J23.